Sep 25th, 11:25 AM

Enhancing High Cycle Fatigue Perfomance Of Electron Beam Melted Ti6Al4V: A Study On Shot Peening And Hot Isostatic Pressing

Naghmeh M. Mojib
University of Washington - Seattle Campus

Dwayne D. Arola
University of Washington - Seattle Campus

Ramulu Mamidala
University of Washington - Seattle Campus

ENHANCING HIGH CYCLE FATIGUE PERFOMANCE OF ELECTRON BEAM MELTED TI6AL4V: A STUDY ON SHOT PEENING AND HOT ISOSTATIC PRESSING

Naghmeh M. Mojib[1], Dwayne Arola[2], and Ramulu Mamidala[1]

[1]Department of Mechanical Engineering, University of Wahington, Seattle WA USA
[2]Department of Material Science Engineering, University of Wahington, Seattle WA USA

Abstract
The qualification of electron beam powder bed fusion (PBF-EB) for safety-critical applications is hindered by variability in high cycle fatigue performance, largely due to surface roughness and internal defects. While Hot Isostatic Pressing (HIP) effectively reduces internal porosity, it does not address surface-initiated fatigue failures. This study investigated the combined effects of HIP and shot peening on enhancing the fatigue performance of PBF-EB Ti6Al4V. Over 50 specimens, including both vertical and horizontal build orientations, underwent high cycle fatigue testing per ASTM E466. X-Ray computed tomography confirmed decrease in defect distribution following HIP, while shot peening resulted in a more uniform surface. Combined HIP and shot peening led to a 100 MPa increase in fatigue compared to machined samples by introducing compressive residual stresses and delaying crack initiation. This study highlights the necessity of integrating combined post-processing strategies in extending the fatigue life of PBF-EB Ti6Al4V.

Keywords Additive Manufacturing, Fatigue Life, Surface Integrity, Post-Processing

Introduction

Monotonic properties of Additive Manufactured (AM) metals are commonly studied; however, knowledge of fatigue behavior is vital for determining a component's durability under cyclic loading. Although static properties of electron beam powder bed fusion (PBF-EB) materials are often comparable to wrought alloys [1], fatigue life remains a fraction of the wrought fatigue endurance limits [2,3]. This discrepancy in cyclic properties is amplified further due to process-induced defects and surface roughness [4], which act as stress concentrators and dominate crack initiation mechanisms. Therefore, understanding the role of these process-induced features on fatigue performance is essential for developing reliable PBF-EB Ti6Al4V components for load-bearing applications.

Among these defects, surface roughness is the primary contributor to early fatigue failure of as-built PBF-EB Ti6Al4V. The poor surface finish originates from (1) the staircase effect from layer-by-layer fabrication, (2) partially sintered powder particles, and (3) surface-connected defects or partially melted areas. While advantageous in biomedical applications for its osteogenic properties [5], this rough surface significantly reduces fatigue strength as low as 150 – 300 MPa [6,7]. Machining has been effective in removing surface and subsurface flaws, improving fatigue life [8], with further improvements up to 450MPa when combined with shot peening through introduction of the beneficial compressive residual stresses [9]. At the same time, internal defects such as lack of fusion (LOF) and gas pores contribute to orientation-dependent fatigue behavior [3,10]. Vertically built samples, despite showing tortuous crack paths and higher crack growth resistance [11], suffer from low fatigue life due to LOF defects aligned perpendicular to the build and loading direction. These finding underscore the need for a combined post-processing strategy that addresses both surface and internal defects– hence the primary motivation leading to this research study.

Hot Isostatic Pressing (HIP) is widely used to reduce internal defects; however, improvements in fatigue performance are only realized when paired with surface treatments such as machining [12]. Although standard HIP at ~920°C effectively heals internal defects, it can degrade the fatigue performance by coarsening the microstructure and reducing crack resistance. Recent studies have shown that subtransus, low temperature HIP can refine microstructure and enhance fatigue behavior, even without complete defect reduction [13]. However, there remains a lack of systematic study combining a subtransus HIP with mechanical surface enhancement, such as shot peening, in PBF-EB Ti6Al4V. The aim of this study is to investigate the effect of an integrated post-processing route -HIP followed by shot peening- on the high cycle fatigue performance of PBF-EB Ti6Al4V. By analyzing build orientation, defect distribution, and surface integrity, this work aims to identify mechanisms governing crack initiation and demonstrate how tailored post-processing can enable the use of metal AM components in critical fatigue-limited applications.

Materials and Methods

The Grade 5 Titanium alloy (Ti6Al4V) powder used in this study was acquired from a General Electric (GE) company subsidiary (Advanced Powders & Coating). The original build began with 100 kg of fresh powder, which was recycled using the Arcam Powder Recovery System (PRS), sieved, and mixed with the powder left in the hoppers. The samples were fabricated on an ARCAM A2X Electron Beam AM system (Mölndal, Sweden) using powder batch #P1143 at the 10th reuse cycle. 10 mm samples were fabricated and machined to the final dimensions shown in Figure 1.

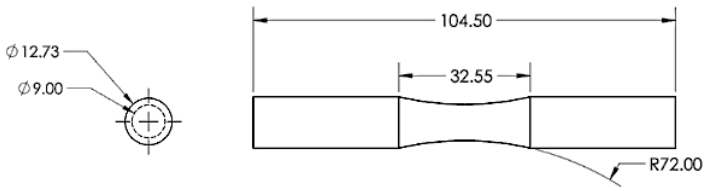

Figure 1. The final dimensions (in mm) per ASTM E466.

Three post-processing treatments were explored in the following study: machining, HIP, and shot peening. The initial set of 38 samples, including both horizontal and vertical orientations, underwent machining and a subsequent low-temperature HIP treatment. A second set of 10 samples in the horizontal orientation underwent machining and shot peening process. The final set of 10 samples in the vertical and horizontal orientation underwent processing in the following order: machining, HIP and shot peen.

The specimens which underwent surface treatment were printed as cylinders and machined to size to ensure dimensional compliance with ASTM E466 [14]. Samples were machined by a local machining vendor (Ballard Machine Works, Seattle, WA) prior to any other surface treatments via a turning process with appropriate parameters for titanium to minimize residual stress buildup. A minimum of 1 mm was removed from the external diameter to insure sufficient removal of the PBF-EB surface and subsurface defects. Shot peening was performed by a local vendor (ASKO Processing, Seattle, WA) per MIL-S-13165. A CW35 shot peen media was used at a .006-.01A intensity at the sample gauge section. A HIP treatment was performed at a lower temperature HIP with high pressure at 815ºC at 190 MPa for 165 min. by Quintus Technologies.

Internal Defect and Surface Characterization

Defect distributions of select specimens were obtained prior to testing using a commercial X-ray microcomputed tomography (µCT) system (X5000, North Star Imaging, Rogers, MN, USA). The projections were created from the scan using commercial software (efX CT) provided by the manufacturer of the µCT system. Appropriate beam hardening corrections were applied during the reconstruction to reduce process-induced artifacts. The projections were imported as an image stack and reconstructed in Volume Graphics VGStudio Max 3.1 for characterizing and

analyzing defects (i.e., diameter, sphericity, location). Two specimens are scanned at a time to reduce scan time and cost without compromising resolution, for a total of six (6) samples.

The surface quality of the as-printed specimens was be obtained prior to testing using the non-contact optical imager (Keyence VR-3100) captures 2D and 3D surface profiles and topography. The values were obtained along the gauge section in the specimens evaluated.

Fatigue Testing

Uniaxial tension-tension high cycle fatigue (HCF) testing was conducted per ASTM E466 [14]. The samples were tested on an Instron hydraulic system (Instron model 8520, Norwood, MA) with a 100kN capacity under constant amplitude with a load ratio (R) of 0.1 at 15 Hz. Minimum of three stress levels between 200 – 800 MPa were selected. The total number of cycles was recorded until failure or an endurance limit of 10^7 cycles is reached. The Basquin power-law relationship was used for fitting.

Fractography

Nikon SMZ1000 (Nikon Metrology Inc., MI, USA) optical microscope and FEI Sirion XL30 (Amsterdam, Netherlands) scanning electron microscopy (SEM) were used to observe the fracture surfaces of HCF specimens. Optical imaging was used for assessing the regions of crack initiation, crack propagation and the area of final rupture of the HCF specimens. The SEM was utilized to obtain finer details of the fracture surfaces and observe possible anomalies leading to reduced mechanical properties.

Results and Discussion

Surface Roughness

The 3D surface morphology is provided in Figure 2 as a function of metal and surface condition. Small defects were observed in the machined samples that underwent a HIP treatment. Lastly, SP samples exhibited a deformed surface due to the shot peening process. However quantitative analysis was required to fully understand the influence of surface roughness.

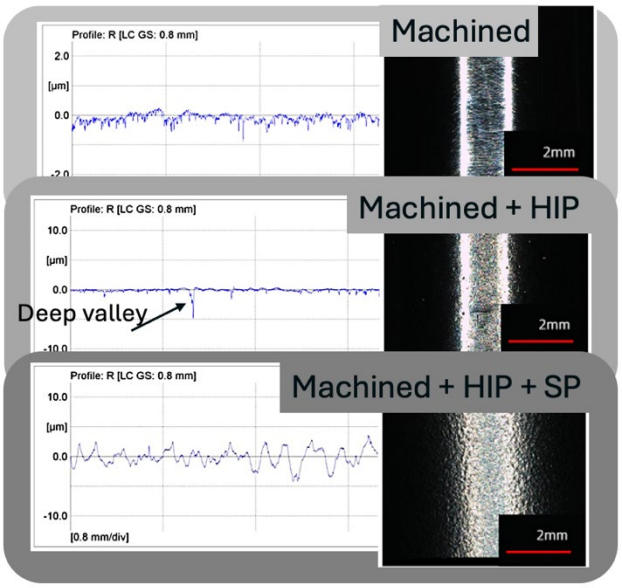

Figure 2. Optical surface morphology

Table 1 summarizes the surface roughness parameters including: the average surface roughness values (R_a), ten-point height (R_z), maximum valley to peak height (R_t), skewness (R_{sk}), and maximum valley depth (R_v), as a function of surface and metal condition. Data of samples in the As-Built condition is included for reference from a previous study [15]. R_a, R_z, R_t, and R_v decreased significantly with machining. The negative R_{sk} values across all conditions indicate valley-dominated surfaces, with an increase in uniformity with shot peening application. Furthermore, it is important to note the significant increase in the scatter in data after the HIP treatment indicating a large range of valleys adorning the surface, as observed in Figure 2.

Table 1. Surface roughness characteristics in each condition

Parameter	As-Built	Machined	Machined + HIP	Machined + HIP + SP
R_a (µm)	24.4 ± 5.6	0.15 ± 0.10	0.22 ± 0.10	0.97 ± 0.14
R_z (µm)	168.5 ± 48.5	0.68 ± 0.08	1.94 ± 0.58	5.42 ±0.71
R_t (µm)	107.6 ± 14.3	11.69 ± 1.48	10.17 ± 2.37	10.78 ± 3.42
R_{sk} (µm)	-0.1 ± 0.10	-1.48 ± 0.11	-2.66 ± 2.48	-0.39 ± 0.31
R_v (µm)	56.5 ± 7.8	5.64 ± 0.59	3.12 ± 0.59	3.89 ± 1.11

Internal Defect Analysis

Figure 3 shows µCT reconstruction and defect trends of PBF-EB Ti6Al4V samples in the *As-Built* and *HIP* condition prior to testing. Non-destructive testing reveals key features of the metal in both conditions. In the as-built samples, two defect types are visible Figure 3 (a): randomly distributed spherical gas pores and irregular high-aspect ratio LOF defects. Defect morphology was quantified using diameter (based on equivalent sphere) and sphericity (ratio of surface area relative to a sphere of equal volume). Sphericity values near 1 indicate spherical pores, while more irregular shapes exhibit lower sphericity. As shown in Figure 3 (c), most defects ranged from 50 µm to 600 µm, with those above 250 µm generally exhibiting low sphericity, corresponding to LOF defects. HIP treatment significantly reduced the number and severity of defects, fully eliminating LOF. While the µCT threshold identified regions of potential internal porosity in HIP samples, no such defects were confirmed upon manual inspection, as shown in Figure 3 (b). Surface-connected defects were excluded from the analysis due to software limitations.

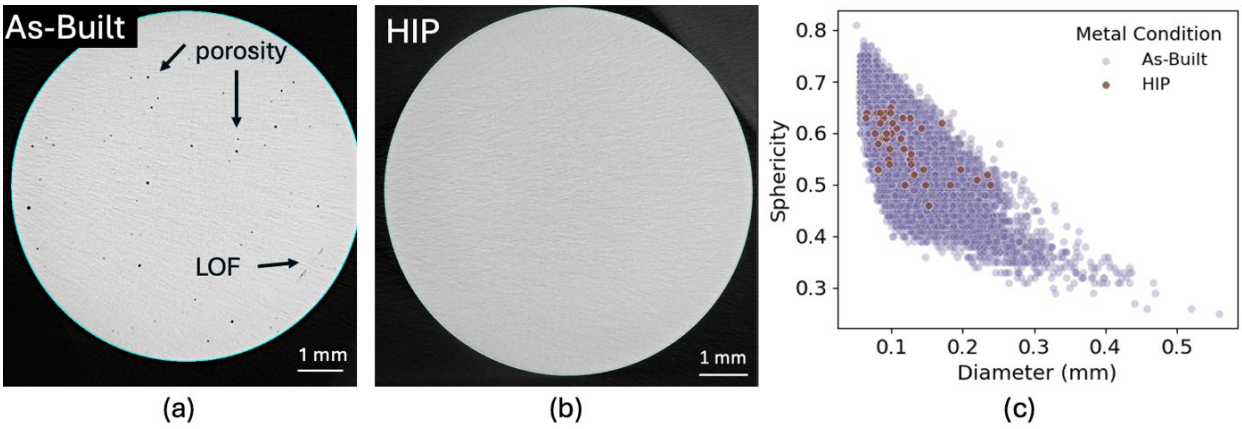

Figure 3. The 3D reconstruction of the internal view of the (a) As-Built and (b) HIP samples. Porosity and LOF defects are observed in the As-Built condition but not HIP. (c) The defect diameter vs. sphericity trends in the as-built and HIP samples.

Tensile Properties

Table 2 summarizes the static mechanical properties in each metal condition, surface, and orientation, including the yield strength (YS), ultimate tensile strength (UTS), elongation, strain hardening, and hardness. Values obtained in the As-Built, HIP, and Machined condition are included for comparison from previous studies [12,15]. The YS and UTS increased by 16% and 15% with the removal of the as-fabricated surface. Similar increase was reported by Schur et al., which was due to the removal of the surface defects formed during the printing process [16]. In

contrast, with the application of HIP and machining, the YS and UTS of the PBF-EB Ti6Al4V exceed wrought alloys [17], in addition to a 40% increase in strain hardening and ~40% increase in elongation. However, with a combination of HIP and machining, studies have found not observed a significant improvement in tensile properties, where the microstructural coarsening from treatment at 920°C often outweighs the benefits of the improved ductility [18,19]. The increase in strain hardening and improved ductility was attributed to the closure of internal defects with the high-pressure HIP process, while the subtransus process temperature limited microstructural changes. As a result, the lower temperature HIP treatment in this study was successful in increasing the metal ductility while maintaining the favorable high strength of the PBF-EB Ti6Al4V.

Table 2. Mechanical properties in each condition

Type	Orientation	Yield Strength (MPa)	Ultimate Tensile Strength (UTS)	Elongation (%)	Strain Hardening
As-Built	Vertical	840	960	9	0.03
HIP	Vertical	852 ± 8	922 ± 9	15.3 ± 1.9	0.04
Machined	Vertical	975 ± 29	1111 ± 36	11.7 ± 2.7	0.05
	Horizontal	997 ± 56	1124 ± 46	10.0 ± 2.8	0.05
Machined + HIP	Vertical	967 ± 9	1028 ± 9	16.9 ± 1.9	0.08
	Horizontal	938 ± 7	1023 ± 13	13.4 ± 2.1	0.07

High Cycle Fatigue

The following section will discuss the various factors influencing PBF-EB fatigue performance. Experimental analysis of PBF-EB in the as-fabricated, surface-treated, and heat-treated condition are evaluated. Figure 4 shows the stress-life curves of post-processed PBF-EB Ti6Al4V as a function of surface and metal condition. The stress-life curves were determined through fitting the experimental data to the Basquin equation for each metal condition and overlayed on published sources for PBF-EB, wrought, and cast Grade 5 Ti6Al4V [15,20,21]. Post-processing significantly enhanced the PBF-EB fatigue performance but heavily depended on the surface condition. Fatigue behavior increased from 200MPa in the As-Built condition to 350MPa with the machining application. Finally, shot peening had the most significant enhancement in fatigue performance, yielding endurance limit up to 400 MPa. In essence, regardless of presence of internal defects, the as-printed surface remained detrimental to the fatigue life of PBF-EB Ti6Al4V. Alternatively, through removal and refinement of the as-printed surface, fatigue life comparable to wrought and cast alloys was achieved.

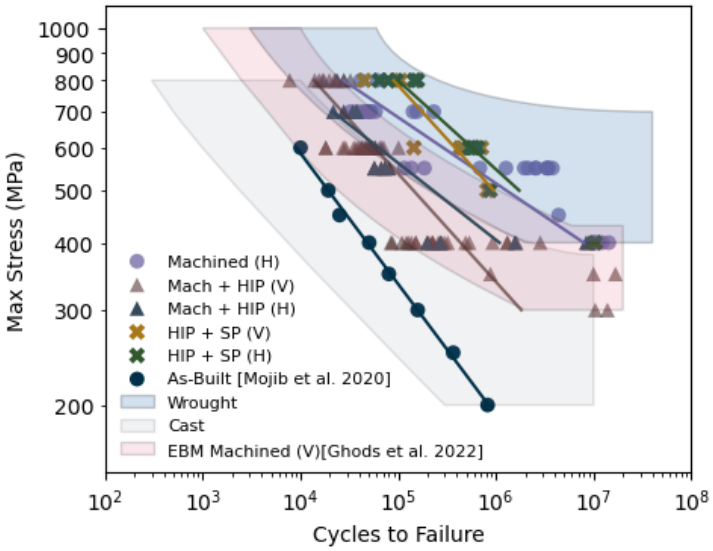

Figure 4. Fatigue stress-life curve as a function of surface and metal condition, in each orientation.

While the surface finish had the most significant influence on the fatigue behavior of PBF-EB Ti6Al4V, further investigation was necessary for understanding factors influencing scatter in the fatigue behavior. The influence of the print orientation on the fatigue behavior of the PBF-EB Ti6Al4V is shown Figure 4. Overall, the horizontal orientation survived longer than the vertical

orientation, with the largest variation in the untreated condition. With an additional application of shot peening, the orientation-dependent fatigue behavior was nearly eliminated. Effectively, the comparable fatigue properties in the two orientations after the shot peening application means that with surface and heat treatment, the largest sources of variation (surface finish, orientation, internal defects) could be reduced.

Fractography

Fractography was performed after sample fracture using optical and scanning electron microscopes. A typical fatigue fracture surface exhibits three distinct regions shown in Figure 5(a): the source of crack initiation, the area of crack propagation and the area of final fracture. Typically, lines are found radiating away from the crack initiation source until it reached a flat fracture region as the crack grows, until the final fracture, where shear lips and ductile dimpling are observed. Spherical gas porosity and LOF defects were only observed on the fracture surface of the untreated sample shown in Figure 5 (b).

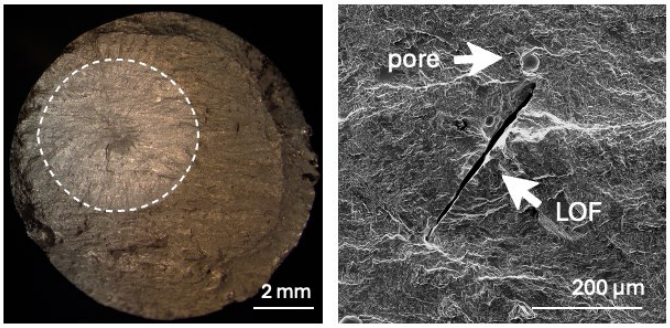

Figure 5. (a) Typical fatigue fracture surface. (b) common defects found in as-built metal.

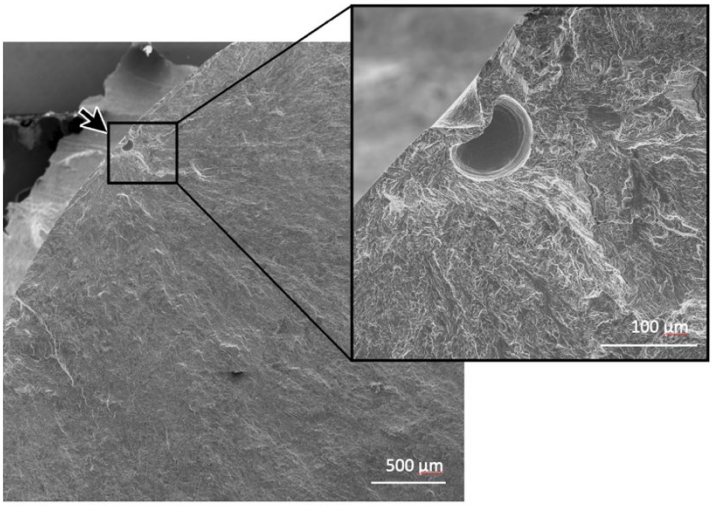

Figure 6. Fractography of the HIP+Machined samples, with the arrows indicate the location of crack initiation.

Figure 6 (a) shows the fracture surface of samples with a HIP treatment. The HIP treatment was successful in removing internal defects, where porosity and LOF defects were not observed on the fracture surface. The subsurface defects located 200μm from the surface with μCT were similarly observed with high-magnification imaging and profilometry. The sharp notch-like defects on the surface of the samples were a result of the high-pressure HIP process deforming preexisting subsurface defects below the external surface. Figure 5(a) exhibits the low magnification fatigue fracture surfaces of the shot peened sample, often failing due to subsurface and internal features.

Fatigue failure originated from three primary nucleation sources: surface, subsurface, and internal defects as shown in **Figure 7**. Failure origins were identified post-fracture and distinguished with the following markers circle (surface), + (subsurface), and X for internal crack nucleation, samples reaching runout at 10^7 cycles are characterized by an arrow. In all as-built specimens, cracks initiated at the surface defects due to the partially melted powder particles, resulting in fatigue limit far below the ~550 MPa reported [6,7,22]. Once the surface was machined, fatigue cracks primarily initiated from subsurface and internal defects. Childerhouse et al. [23] showed fatigue strength doubled when 1mm of surface material was removed, highlighting the critical role of removing both surface and subsurface defects.

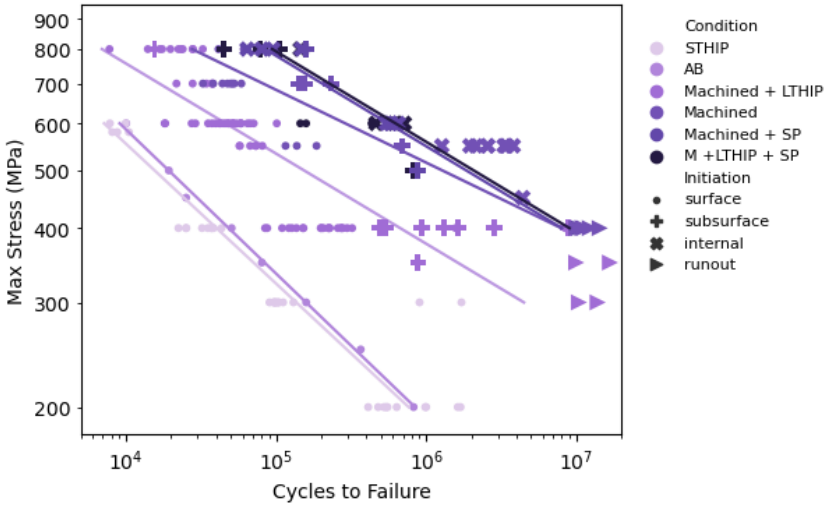

Figure 7. Summary of crack nucleation source of samples for each metal and surface condition.

Although surface roughness had the most significant influence on the fatigue behavior, the LOF defects continued to degrade performance and introduce variability. Zhang et al. [24] demonstrated that even when crack initiated from surface defects, process-induced internal defects still influenced the fatigue performance of Ti6Al4V. Large and irregularly shaped internal defects increase the overall stress intensity and reducing the load-carrying capacity, especially when aligned perpendicular to the loading direction commonly observed in the vertical orientation. In contrast, the horizontally-oriented Ti6Al4V, with less critical LOF, exhibited fatigue lives 5X the vertical orientation, reaching runout at 400MPa. However, with HIP application, the Machined samples also did not result in enhanced fatigue performance shown in Figure 7. Fractography and surface characterization revealed persistent surface valleys and imperfections in these samples, likely introduced due to the order of post-processing. However, with the application of shot-peening, these subsurface defects were compressed, with the crack initiation shifting to internal defects. This suggests applying HIP after machining may induce sharp notch-like defects that act as critical stress concentration, ultimately limiting fatigue performance despite the combined treatment.

This work encompassed samples printed systematically to evaluate post-processing of the fatigue life of PBF-EB Ti6Al4V. Over 50 samples were tested in the machined, HIP and shot peened condition and two orientations to understand the repeatability and reliability of the metal. The post-processing treatment had the largest influence on the fatigue behavior, where shot peening reported values nearly twice those in the untreated condition. While HIP was successful in reducing internal porosity and defects, the subsurface defects remained and were the source of crack initiation. Shot peening however was successful in reducing the orientation-dependent behavior and reducing scatter in the data. Additional samples and chemical analysis of the metal are recommended to better understand the remaining variation in the shot peened metal. The integrated post-processing of PBF-EB Ti6Al4V alloy was promising for adoption, where with the

application of machining, HIP, and shot peening, metal comparable to annealed wrought Ti6Al4V can be achieved.

Conclusion

AM offers exciting advantages for fabricating complex and unique shapes, but it's widespread adoption for structural applications requires a thorough understanding of fatigue behavior. This study investigated the effects of post-processing on the fatigue performance of PBF-EB Ti6Al4V, leading to the following key conclusions:

1. Hot Isostatic Pressing at 815°C was successful in reducing internal defects, resulting in yield and ultimate tensile strengths comparable to the untreated metal, while enhancing elongation by approximately 40%.
2. Surface roughness was the dominant factor influencing fatigue performance, followed by build orientation effects, where horizontally built samples consistently outperformed vertical orientation. The orientation effects reduced with the integrated post-processing approach.
3. Fatigue behavior increased with post-processing applications, with the combined post-processing (Machined+ HIP+SP) as the most promising treatment, resulting in fatigue behavior comparable to wrought annealed Ti6Al4V. However, performing machining prior to HIP resulted in subsurface defects creating sharp surface notches that acted as the source of crack initiation, limiting fatigue behavior.

These results demonstrate that PBF-EB Ti6Al4V can be a viable material for structural applications, provided that a carefully optimized post-processing route – consisting of low-temperature HIP, machining, and shot peening (in that order) – is employed to mitigate defects and enhance fatigue resistance.

References

[1] H.D. Nguyen, A. Pramanik, A.K. Basak, Y. Dong, C. Prakash, S. Debnath, S. Shankar, I.S. Jawahir, S. Dixit, D. Buddhi, *A critical review on additive manufacturing of Ti-6Al-4V alloy: microstructure and mechanical properties*, Journal of Materials Research and Technology 18 (2022) 4641–4661. https://doi.org/10.1016/J.JMRT.2022.04.055.

[2] Y.Y. Sun, S.L. Lu, S. Gulizia, C.H. Oh, D. Fraser, M. Leary, M. Qian, *Fatigue Performance of Additively Manufactured Ti-6Al-4V: Surface Condition vs. Internal Defects*, JOM 72 (2019). https://doi.org/10.1007/s11837-020-04025-7.

[3] S. Tammas-Williams, P.J. Withers, I. Todd, P.B. Prangnell, *The Influence of Porosity on Fatigue Crack Initiation in Additively Manufactured Titanium Components*, Sci Rep 7 (2017). https://doi.org/10.1038/s41598-017-06504-5.

[4] D. Greitemeier, C. Dalle Donne, F. Syassen, J. Eufinger, T. Melz, *Effect of surface roughness on fatigue performance of additive manufactured Ti–6Al–4V*, Materials Science and Technology (United Kingdom) 32 (2016) 629–634. https://doi.org/10.1179/1743284715Y.0000000053.

[5] L. Liu, S. Wang, J. Liu, F. Deng, Z. Li, Y. Hao, *Architectural design of Ti6Al4V scaffold controls the osteogenic volume and application area of the scaffold*, Journal of Materials Research and Technology (2020). https://doi.org/10.1016/j.jmrt.2020.11.061.

[6] A.H. Chern, P. Nandwana, T. Yuan, M.M. Kirka, R.R. Dehoff, P.K. Liaw, C.E. Duty, *A review on the fatigue behavior of Ti-6Al-4V fabricated by electron beam melting additive*

manufacturing, Int J Fatigue 119 (2019) 173–184. https://doi.org/10.1016/j.ijfatigue.2018.09.022.

[7] D. Greitemeier, F. Palm, F. Syassen, T. Melz, *Fatigue performance of additive manufactured TiAl6V4 using electron and laser beam melting*, Int J Fatigue 94 (2016) 211–217. https://doi.org/10.1016/j.ijfatigue.2016.05.001.

[8] T. Persenot, J.Y. Buffiere, E. Maire, R. Dendievel, G. Martin, Fatigue properties of EBM as-built and chemically etched thin parts, in: Procedia Structural Integrity, Elsevier B.V., Lecco, 2017: pp. 158–165. https://doi.org/10.1016/j.prostr.2017.11.073.

[9] H. Soyama, F. Takeo, *Effect of various peening methods on the fatigue properties of Titanium alloy Ti6Al4V manufactured by direct metal laser sintering and electron beam melting*, Materials 13 (2020). https://doi.org/10.3390/ma13102216.

[10] Y. Nadot, *Fatigue from Defect: Influence of Size, Type, Position, Morphology and Loading*, Int J Fatigue 154 (2022) 106531. https://doi.org/10.1016/J.IJFATIGUE.2021.106531.

[11] R. VanSickle, D. Foehring, H.B. Chew, J. Lambros, *Microstructure effects on fatigue crack growth in additively manufactured Ti–6Al–4V*, Materials Science and Engineering: A 795 (2020) 139993. https://doi.org/10.1016/J.MSEA.2020.139993.

[12] M. Mojib, H. Soyama, D. Sanders, D. Arola, M. Ramulu, *The High Cycle Fatigue Behavior of Surface Treated Electron Beam Melted Titanium Ti6Al4V*, International Mechanical Engineering Congress and Exposition IMECE2021 (2022) 71975. https://doi.org/10.1115/IMECE2021-71975.

[13] T.P. Moran, P.E. Carrion, S. Lee, N. Shamsaei, N. Phan, D.H. Warner, *Hot Isostatic Pressing for Fatigue Critical Additively Manufactured Ti-6Al-4V*, Materials 2022, Vol. 15, Page 2051 15 (2022) 2051. https://doi.org/10.3390/MA15062051.

[14] ASTM E466-21: Standard Practice for Conducting Force Controlled Constant Amplitude Axial Fatigue Tests of Metallic Materials, West Conshohocken, PA, 2021. https://doi.org/10.1520/E0466-21.

[15] M. Mojib, R. Pahuja, M. Ramulu, D. Arola, High Cycle Fatigue Behavior of Recycled Additive Manufactured Electron Beam Melted Titanium Ti6Al4V, in: International Mechanical Engineering Congress and Exposition IMECE2020, ASME, Portland, 2020: p. 24194.

[16] R. Schur, S. Ghods, C. Wisdom, R. Pahuja, A. Montelione, D. Arola, M. Ramulu, *Mechanical anisotropy and its evolution with powder reuse in Electron Beam Melting AM of Ti6Al4V*, Mater Des 200 (2021) 109450. https://doi.org/10.1016/J.MATDES.2021.109450.

[17] ASM Handbook, Fatigue and Fracture, ASM International, 1996. https://doi.org/10.31399/ASM.HB.V19.A0002409.

[18] A. Abu-Issa, M. Lopez, C. Pickett, A. Escarcega, E. Arrieta, L.E. Murr, R.B. Wicker, M. Ahlfors, D. Godfrey, F. Medina, *Effects of altered hot isostatic pressing treatments on the microstructures and mechanical performance of electron beam melted Ti-6Al-4V*, Journal

of Materials Research and Technology 9 (2020) 8735–8743. https://doi.org/10.1016/J.JMRT.2020.06.019.

[19] K. Thalavai Pandian, M. Neikter, F. Bahbou, T. Hansson, R. Pederson, *Elevated-Temperature Tensile Properties of Low-Temperature HIP-Treated EBM-Built Ti-6Al-4V*, Materials 2022, Vol. 15, Page 3624 15 (2022) 3624. https://doi.org/10.3390/MA15103624.

[20] ASM Handbook, Properties and Selection: Nonferrous Alloys and Special-Purpose Materials, ASM International, Novelty, OH, USA, 1990. https://doi.org/10.31399/ASM.HB.V02.9781627081627.

[21] S. Ghods, R. Schur, A. Montelione, R. Schleusener, D.D. Arola, M. Ramulu, *Importance of Build Design Parameters to the Fatigue Strength of Ti6Al4V in Electron Beam Melting Additive Manufacturing*, Materials 15 (2022) 5617. https://doi.org/10.3390/ma15165617.

[22] S. Franchitti, C. Pirozzi, R. Borrelli, *Influence of hot isostatic pressing and surface finish on the mechanical behaviour of Ti6Al4V processed by electron beam melting*, Fatigue Fract Eng Mater Struct 43 (2020) 2828–2841. https://doi.org/10.1111/ffe.13295.

[23] T. Childerhouse, E. Hernández-Nava, N. Tapoglou, R. M'Saoubi, L. Franca, W. Leahy, M. Jackson, *The influence of finish machining depth and hot isostatic pressing on defect distribution and fatigue behaviour of selective electron beam melted Ti-6Al-4V*, Int J Fatigue 147 (2021) 106169. https://doi.org/10.1016/j.ijfatigue.2021.106169.

[24] J.S. Zhang, Y.T. Tang, R. Jin, A. Lui, P.S. Grant, E. Alabort, A.C.F. Cocks, R.C. Reed, *On the size-dependent fatigue behaviour of laser powder bed fusion Ti-6Al-4V*, Addit Manuf 79 (2024) 103922. https://doi.org/10.1016/J.ADDMA.2023.103922.